ISSN 1064-2269, Journal of Communications Technology and Electronics, 2015, Vol. 60, No. 10, pp. 1124–1133. © Pleiades Publishing, Inc., 2015.
Original Russian Text © P.V. Lega, V.V. Koledov, D.S. Kuchin, P.V. Mazaev, A.M. Zhikharev, A.V. Mashirov, V.S. Kalashnikov, S.A. Zybtsev, V.Ya. Pokrovskii, V.G. Shavrov, V.A. Dikan, L.V. Koledov, A.V. Shelyakov, A.V. Irzhak, 2015, published in Radiotekhnika i Elektronika, 2015, Vol. 60, No. 10, pp. 1080–1089.

PHYSICAL PROCESSES IN ELECTRON DEVICES

Simulation of the Control Process Applied to the Micromechanical Device with the Shape Memory Effect

P. V. Lega[a], V. V. Koledov[a], D. S. Kuchin[a], P. V. Mazaev[a], A. M. Zhikharev[a], A. V. Mashirov[a], V. S. Kalashnikov[a], S. A. Zybtsev[a], V. Ya. Pokrovskii[a], V. G. Shavrov[a], V. A. Dikan[b], L. V. Koledov[c], A. V. Shelyakov[d], and A. V. Irzhak[e]

[a] *Kotel'nikov Institute of Radio Engineering and Electronics, Russian Academy of Sciences, ul. Mokhovaya 11, building 7, Moscow, 125009 Russia*

[b] *National University of Science and Technology (MISIS), Leninskii pr. 4, Moscow, 119991 Russia*

[c] *Don State Technical University, pl. Gagarina 1, Rostov-on-Don, 344000 Russia*

[d] *National Research Nuclear University MEPhI (Moscow Engineering Physics Institute), Kashirskoe sh. 31, Moscow, 115409 Russia*

[e] *Institute of Microelectronics Technology and High Purity Materials, Russian Academy of Sciences, ul. Akademika Osip'yana 6, Chernogolovka, Moscow oblast, 142432 Russia*

e-mail: shavrov@cplire.ru; victor_koledov@mail.ru

Received December 22, 2014

Abstract—It has recently been proved that, in alloys, e.g., based on the Ti–Ni system, a shape memory effect (SME) is preserved down to the nanoscale sizes of an active alloy layer and demonstrated ultrasmall-sized and fully functional micro- and nanomechanical devices: actuators and nanotweezers that are fabricated via standard microelectronic technologies relying on composite materials with the SME. In the nearest future, such achievements will enable the creation of the next-generation micro- and nanomechanical devices whose sizes are quite comparable with those inherent to, e.g., carbon nanotubes, graphene sheets, viruses, etc. Mathematical simulation methods are used to study how the shape-memory micromechanical devices can be activated by means of resistive pulse heating. A decrease in the overall sizes of heating elements (from 1 mm to 10 μm) is demonstrated to be accompanied by the fact that the speed of operation increases sharply from 10^2 to 10^5 s^{-1} and, simultaneously, the energy consumption diminishes from 10^{-3} to 10^{-8} J per operation. The preliminary results of experiments whereby the control of the composite nanotweezer exhibiting the SME is perfected with the help of the automatic pulsed heating technology, as well as the prospects for creating high-speed and high-performance microrobotic systems incorporating newly developed components, are discussed.

DOI: 10.1134/S1064226915100083

INTRODUCTION

Over the last few years, progress in producing new materials has stimulated fast achievements in various fields of microelectronics and microsystem technology. Alloys with a shape memory effect (SME) belong to an important class of heat-controlled functional materials ensuring giant (up to 10%) deformations. In recent years, shape-memory alloy technology has been rapidly developed. In particular, it was revealed that the novel nanostructure substantially increases substantially both the operational and functional properties of shape-memory alloys [1]. In ferromagnetic allows, an opportunity of controlling the SME was demonstrated by switching on/off a magnetic field at constant temperatures [2–7]. It has recently been proved that, e.g., in Ti–Ni, Ti–Ni–Cu, and Ni_2MnGa alloys, the SME remains intact down to submicro- and nanometer sizes of an active alloy layer [8–16]. Standard technologies of local ion etching and ion-induced deposition from a gas phase made it possible to fabricate ultrasmall-sized micro- and nanomechanical devices: nanotweezers with the SME. Their operational capability was successfully demonstrated during manipulations with real micro- and nanometer-sized objects, such as carbon nanotubes, sets of graphene sheets, microbiofibers, and microparticles.

Below, mathematical simulation methods are employed to study how the new-generation micromechanical devices exhibiting the SME can be activated via pulsed resistive heating. The goal of this work is to investigate the energy and time characteristics of the control system versus the heating system sizes, experimentally test the prototype of the system whereby a micromechanical device can be automatically controlled by means of pulsed heating, and discuss the prospects for creating the high-speed and high-performance microrobotic systems based on newly developed components.

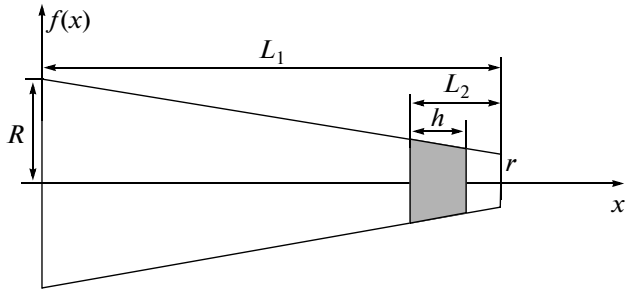

Fig. 1. SME microdevice control model. The heater is designed as a tapered needle with the resistive heating element located near its thin end. Here, R and r are, respectively, the radii of thick and thin needle ends; L_1 is the needle length; L_2 is the distance between the beginning of the heating element and the needle tip, and h is the resistive heating-element length. The heater model is scaled using the equality $L_2 = 2h$.

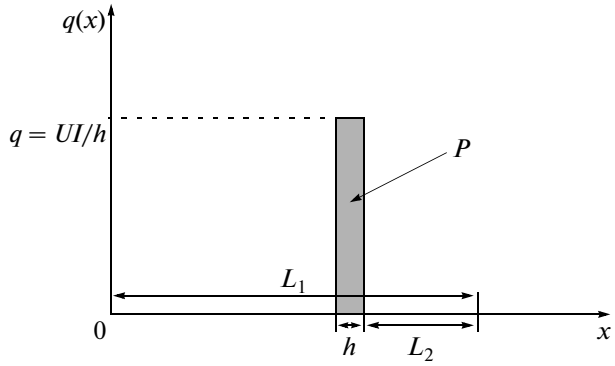

Fig. 2. Dependence of the heating-power density $q(x)$ on the coordinate x. Here, $P = UI$ and h are, respectively, the heating-element power and its length; L_1 is the needle length; and I and U are, respectively, the current flowing through the heating element and the voltage over it.

1. MATHEMATICAL MODEL DESCRIBING THE CONTROL PROCESS APPLIED TO MICROMECHANICAL DEVICES WITH THE SHAPE MEMORY EFFECT

A. Physical Model of the Control Process

The purpose of the model-based system is to govern a micromechanical device, nanotweezer, described in [8–16]. The nanotweezer involves a bimetallic composite material consisting of SME and elastic layers. The main physical effect underlying any SME device is a thermoelastic martensitic transformation of the first order. During a direct martensitic transition, the cooling process is associated with the fact that a cubic high-temperature alloy phase, austenite, converts into a low-symmetry low-temperature phase, martensite. Similar to the first-order phase transition, thermoelastic martensitic transformation is characterized by a temperature hysteresis. Below, it is assumed that M_s and M_f are, respectively, the starting and final temperatures of direct martensitic transition and A_s and A_f are, respectively, the starting and final temperatures of reverse martensitic transition. The given work deals with Ti_2NiCu alloy for which M_s, M_f, A_s, and A_f are 42, 39, 50, and 52°C, respectively [16].

The nanotweezer, the sizes and heat capacity of which are negligibly small, is located at the pointed tip of a tapered microwire (Fig. 1). The thicknesses of thin and thick microwire ends are, respectively, 1 μm or less and 0.5 mm, and its length is $L \approx 1$ cm. The thin end does not emit heat because the nanotweezer is immersed in vacuum. The thick microwire end is maintained at fixed (room) temperature T_0. The resistive-heating element, e.g., diode or thermistor, has length h and is arranged at distance L_2 from the pointed tip. Thus, the minimum distance between the pointed microwire tip and the heating element is $L_1 - h$. The heat capacity of the heating element is disregarded.

The nanotweezer actuation (closing) criterion is defined as $T_1 > A_f$; i.e., the thin microwire tip is heated to the temperature exceeding that corresponding to the termination of the martensite–austenite transition in the SME alloy. The opening criterion is written as $T_2 < M_f$; i.e., the pointed microwire tip is cooled to the temperature less than that observed at the end of the martensite–austenite transition in the SME alloy (see details in [13, 14]). It is commonly supposed that, along the entire length of the heater, the technological restriction of the temperature $T < 400$ K.

B. Generalized 1D Problem of Heat Transfer along the Variable Cross-Section Rod

On the basis of the energy balance equation, the differential heat conduction equation can be written as [17, 18]

$$\rho C f(x)\frac{\partial T}{\partial t} = \frac{\partial}{\partial x}\left(\lambda\frac{\partial T}{\partial x}f(x)\right) + q(x), \quad (1)$$

$$f(x) = \pi\left(\frac{R-r}{L_1}x + R\right)^2, \quad (2)$$

where C is the heat capacity; ρ is the density; λ is the thermal conductivity of a needle material; R and r are, respectively, the thick and thin needle ends; and $f(x)$ is the tapered-needle cross section as a function of coordinate x. A heating source is a diode or thermistor. In calculations, the heating source is simulated by a needle region of length h, in which specific heat power q is homogeneous along the needle length (Fig. 2). Thus, the whole heater power is $P = qh$. Substituting (2) into (1) and performing differentiation, we obtain

$$\rho C\frac{\partial T}{\partial t} = \frac{\partial}{\partial x}\left(\lambda\frac{\partial T}{\partial x}\right) + \lambda\left(\frac{\partial T}{\partial x}\right)\left[\frac{2(R-r)}{(R-r)x + RL_1}\right] + \frac{q(x)}{\pi\left(\frac{R-r}{L_1}x + R\right)^2}. \quad (3)$$

The boundary conditions are defined as

$$\frac{\partial T}{\partial x} = 0 \text{ at } x = L_1, \quad (4)$$

$$T(x = 0) = T_0. \quad (5)$$

The initial condition is written as

$$T(x, t = 0) = T_0. \quad (6)$$

In calculations, it is customary to assume that the microwire material is tungsten, the heat capacity, density, thermal conductivity of which are, respectively, $C = 134$ J/(kg K), $\rho = 19250$ kg/m^3, and $\lambda = 162.8$ W/(m K); $R = 0.25 \times 10^{-3}$ m is the thick-needle-end radius; $r = 0.5 \times 10^{-6}$ m is the thin-needle-end radius; $L_2 = 2h$ is the distance between the starting edge of the heating element and the needle tip (h is the heating-element length); $L = 10^{-2}$ m is the needle length; P is the heater power; and $T_0 = 293.15$ K.

Calculations were carried out using the physical model under the following assumptions:

(i) Temperature distributions over the coordinate and in time are evaluated versus the heater power P. The minimum time intervals required for the heat-insulated thin tip of the heater needle to be heated up to the nanotweezer actuation temperature $T_1 = 350$ K and cooled down to the opening temperature $T_2 = 320$ K are determined. Under the initial conditions, the microwire temperature is $T_0 = 293.15$ K and the nanotweezer is opened.

(ii) Calculations are performed at different values of h. In this case, the problem geometry is proportionally scaled so that the distance between a terminal heater edge and a pointed microwire tip remains equal to the heating-element width h (i.e., $L_2 = 2h$) under changes in scale parameter h.

(iii) A single current pulse is employed.

(iv) The dependences of the nanotweezer actuation time t_{pl} and the energy $W = Pt_{pl}$ on the scale parameter h are calculated at quantities h varying from 10^{-3} to 10^{-5} m.

(v) In the problem under consideration, the technologically restriction imposed on the heater power is caused by the fact that the heater temperature must not exceed 400 K. This restriction is typical of silicon diodes and other materials used in electronic technology. The maximum power needed to satisfy the given condition is also determined during numerical simulation.

C. Numerical Calculation Results

Calculations were performed using MATLAB and COMSOL program packages and provided approximately identical results.

The numerical calculation results are presented as graphs illustrating the dependences of the heater needle temperature on the coordinate at different time values. Dependences between the heater needle temperature and the coordinate, which were obtained at $h = 1000$ μm, $L_2 = 2000$ μm, $P = 285$ mW, and $t = 0$–3.5 ms, are depicted in Fig. 2. The heating process ceases at the heater temperature $T = 395$ K, corresponding to the instant $t_{pl} = 6.5$ ms (Fig. 3, curve *5*). After cessation of heating, i.e., at $t > t_{pl} = 6.5$ ms, (Fig. 3, curves *6*–*10*), the tip temperature grows to 386 K and then reduces to 320 K at instant $t = t_c = 35$ ms, indicating that the complete closing–opening cycle occurs. Thus, the nanotweezer closing time (i.e., the time it takes for the needle tip to be heated to $T = 386$ K) is t_{pl}, and its opening time (i.e., the times required for the needle tip to be cooled to $T = 320$ K) corresponds to t_c. The power was selected so that the nanotweezer actuated within the shortest time without violation of the technological restriction on the maximum temperature of the heating element.

Figure 4 presents the dependences of the temperature on the coordinate obtained at $h = 100$ μm, $L_2 = 200$ μm, $P = 30$ mW, and $t = 0$–440 μs. On the basis of calculations, it was found that $t_{pl} = 83$ μs and $t_c = 44$ μs.

Figure 5 depicts the dependences of the temperature on the coordinate obtained at $h = 10$ μm, $L_2 = 20$ μm, $P = 9$ mW, and $t = 0$–9 μs. As a result of calculations, it was ascertained that $t_{pl} = 1.4$ μs and $t_c = 9$ μs.

Figure 6 graphically characterizes the scaling of the energy W and t_{pl} calculated versus h. The dependence between the calculated allowable heater power P and the scale parameter h is illustrated in Fig. 7. In the log-log scale, calculated dependences $W(h)$, $t_{pl}(h)$, and $P(h)$ are almost linear, corresponding to power-law variations (Fig. 8). The slope ratio determined via the least-squares method is $k = 2.59$. Accordingly, we obtain

$$W \sim h^{-2.59}, \quad (7)$$

$$t_{pl}(h) \sim h^{-2.59}, \quad (8)$$

$$P(h) \sim h^{-1}. \quad (9)$$

The heating-system scaling is specified by dependences (7)–(9), making it possible to predict control-system properties in the pulse mode if sizes vary proportionally. In practice, the scale parameter h, as well as the technological criterion that imposes constraints on the maximum heater temperature, is determined by manufacturing capabilities. Under pulsed heating conditions, relationships (7)–(9) indicate that both actuation time and energy consumption diminish sharply with deceasing scale parameter h.

Note that, in scaling applied to the given model, an increase in the speed of operation is an obligatory but insufficient condition because there are no experimental data confirming that the SME and a martensitic transition can appear in the time interval of 10^3 s or less. With the aim at proving the opportunity of creat-

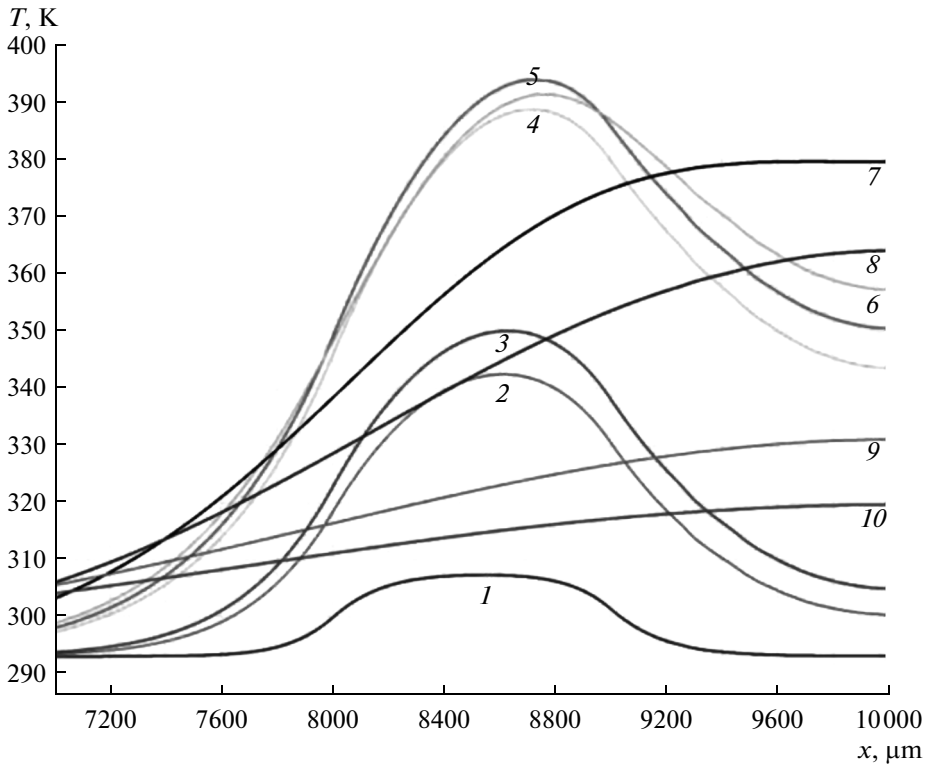

Fig. 3. Dependences between the heater needle temperature and the coordinate obtained at $h = 1000$ μm, $L_2 = 2000$ μm, $P = 285$ mW, and $t =$ (*1*) 0.0006, (*2*) 0.0025, (*3*) 0.003, (*4*) 0.006, (*5*) 0.0065, (*6*) 0.007, (*7*) 0.01, (*8*) 0.015, (*9*) 0.0265, and (*10*) 0.035 s. The heating process ceases at the instant corresponding to the heating-element temperature $T = 395$ K.

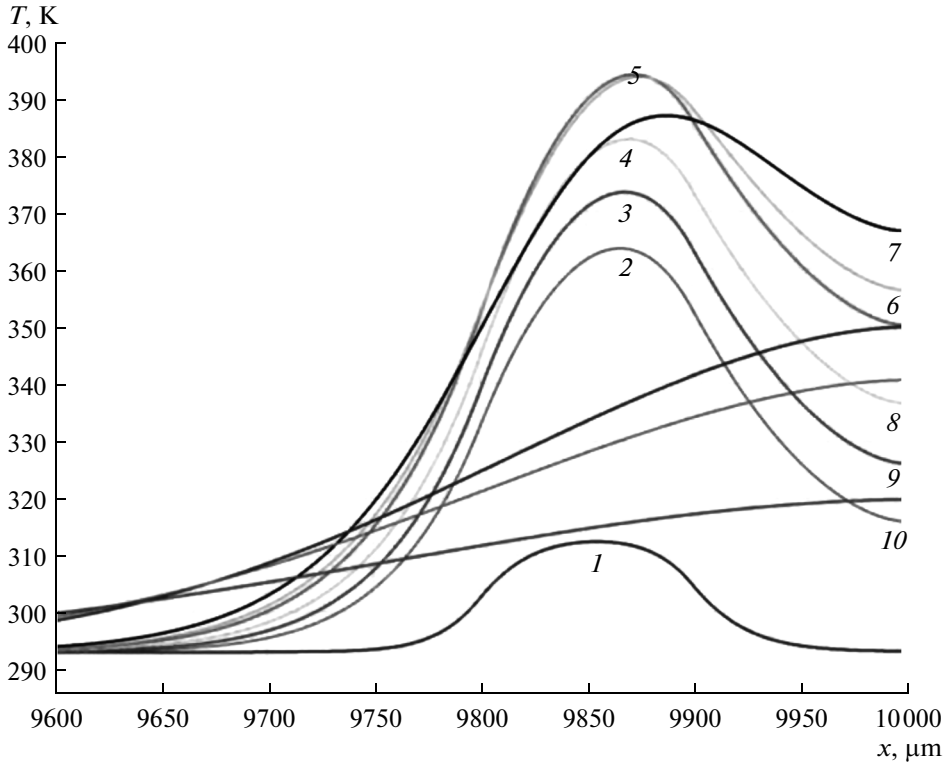

Fig. 4. Dependences between the heater needle temperature and the coordinate obtained at $h = 100$ μm, $L_2 = 200$ μm, $P = 30$ mW, and $t =$ (*1*) 10, (*2*) 50, (*3*) 60, (*4*) 70, (*5*) 83, (*6*) 89, (*7*) 100, (*8*) 240, (*9*) 280, and (*10*) 440 μs. The heating process ceases at the instant corresponding to the heating-element temperature $T = 395$ K.

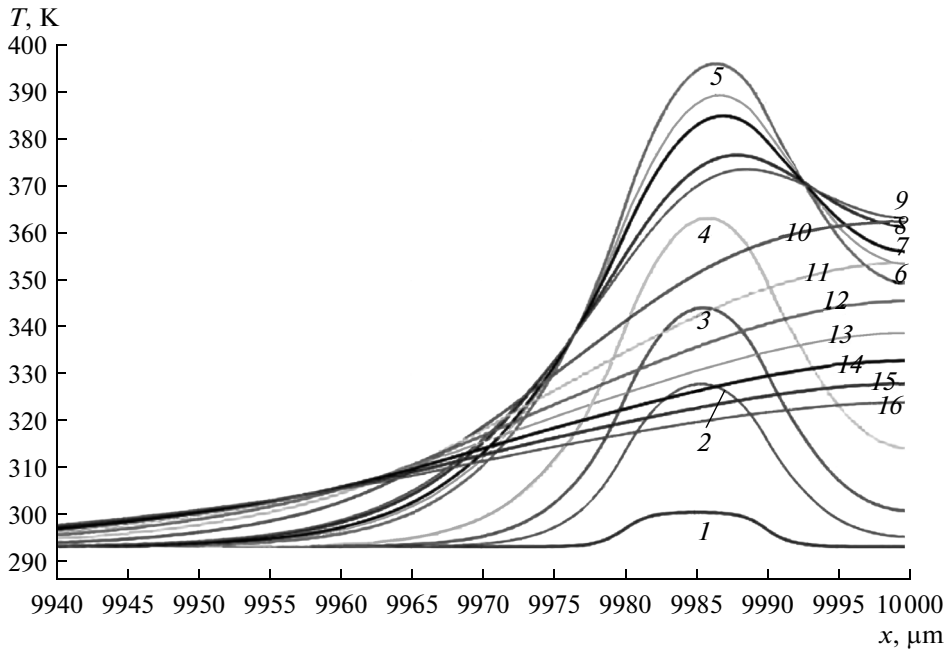

Fig. 5. Dependences of the temperature on the coordinate obtained at $h = 10$ μm, $L_2 = 20$ μm, $P = 9$ mW, and $t =$ (*1*) 0.005, (*2*) 0.03, (*3*) 0.05, (*4*) 0.08, (*5*) 0.14, (*6*) 0.16, (*7*) 0.17, (*8*) 0.19, (*9*) 2, (*10*) 3, (*11*) 4, (*12*) 5, (*13*) 6, (*14*) 7, (*15*) 8, and (*16*) 9 μs. The heating process ceases at the instant corresponding to the heating-element temperature $T = 395$ K.

ing high-speed and high-performance micromechanical devices, which allow for not only an acceleration in heat exchange but also the dynamics of the austenite–martensite phase boundary and changes (associated with its motion) in the shape of small-sized alloy samples, it is necessary to perform deep experimental investigations, which can require the development of new SME alloys, techniques of fabrication of micrometer-sized objects, and new experimental methods of the study thereof.

2. EXPERIMENTAL

A. Scheme of the Automatic Pulsed Control of the Heating Process

The prototype system whereby a nanotweezer can be resistively heated in the automatic pulsed mode was fabricated and investigated in the chamber of a FEI FIB Strata 201 focused ion-beam microscope. The electronic schematic diagram of the setup designed to

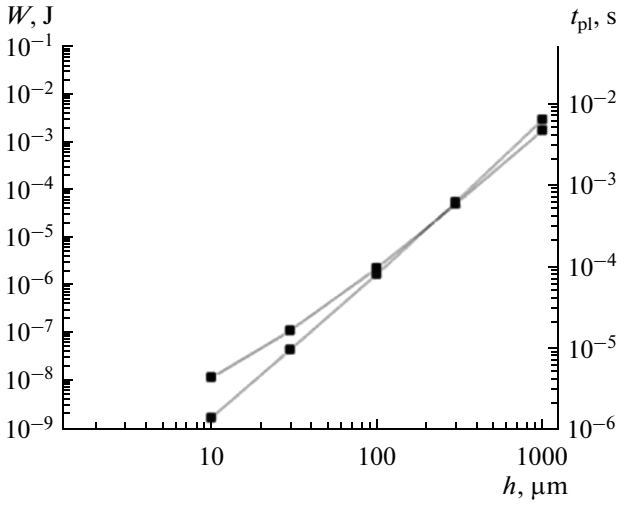

Fig. 6. Dependences of the energy W required for nanotweezer actuation and closing time t_{pl} on the parameter h.

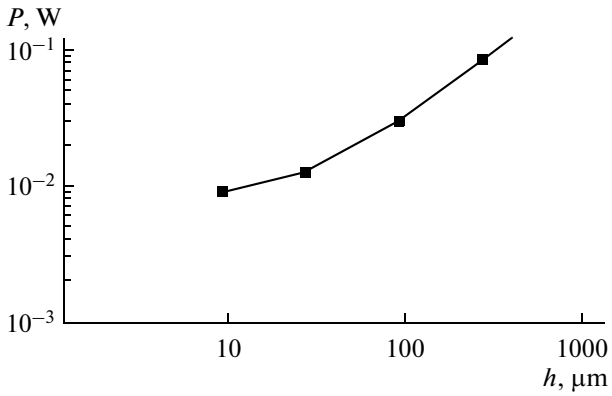

Fig. 7. Dependence of the power P restricted by technological requirements on the scale parameter h.

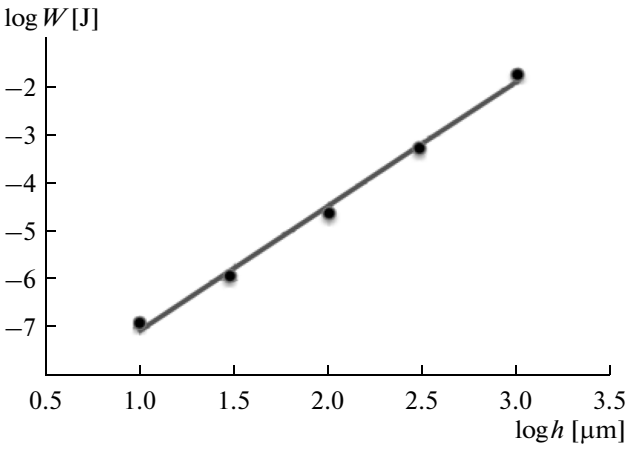

Fig. 8. Dependence between the logarithmic energy W needed for the needle tip to be heated to a temperature of 350 K and the logarithmic heater width h (point). The least-squares approximation of energy values is shown by the straight-line segment.

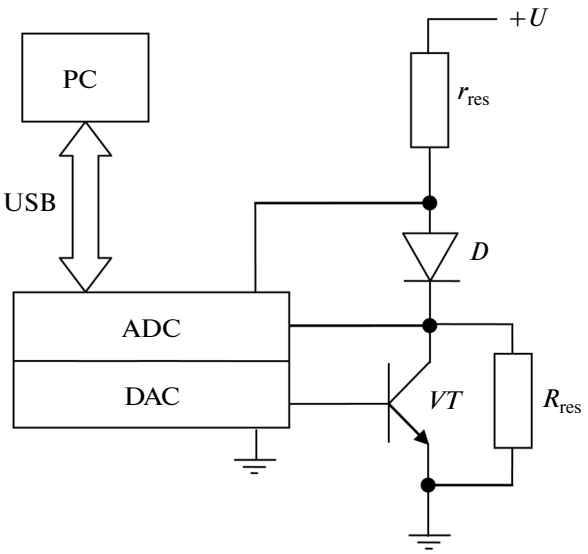

Fig. 9. Schematic diagram of the setup designed to control the pulsed heating process.

control the heating of the needle with the attached nanotweezer is depicted in Fig. 9.

The setup operates as follows. Diode D is mounted near the needle tip. When transistor VT is driven to cutoff, the circuit current flows through both resistor r_{res} and diode D and resistor R_{res} of large resistance ($R_{res} > r_{res}$). In this case, the current is small and the diode temperature increases inappreciably. The diode voltage is measured with the help of the ADC board. At the fixed current, the voltage across diode D (i.e., the chosen 2D910B1 diode chip) depends on its temperature. Thus, the diode temperature can be calculated after this dependence is preliminarily studied. When transistor is driven to connection by means of a DAC signal, the current restricted by resistor r_{res} flows through the diode. The resistor r_{res} prevents the burnout thereof. In this case, the current becomes appreciable and leads to diode and needle heating.

Thus, the setup operation cycle is divided into two time intervals of equal duration, in which measurements and expectable heating are carried out. If the diode temperature turns out to be less than that of the reliable nanotweezer actuation in the measurement interval, the DAC signal is applied to the transistor in the next interval. As a result, the circuit current grows and the diode is heated. If the temperature is large enough to sustain the nanotweezer in the closed state, a pulse is not applied. The timing diagrams illustrating the principles of pulsed control of the nanotweezer heater temperature are presented in Fig. 10.

The composite nanotweezer control system was experimentally tested under pulse-periodic conditions. The time dependence of the heating-element diode voltage is depicted in Fig. 9. During the experiment, the operation cycle was divided into two (measurement and probable heating) intervals with equal durations of 60 ms. Under exposure to heating-pulse trains, the diode is heated and, consequently, its voltage decreases over the time interval of measurements (Fig. 11). Upon attaining the working temperature T_1, which corresponds approximately to a 0.1-V drop across the diode, the average diode voltage is stabilized near 0.1 V (horizontal line) because the frequency reduces automatically and heating current pulses are supplied. The system exhibited the reliable control process, and the nanotweezer actuation time was less than 1 s.

B. Results of Experiments on the Manipulation of Nanometer-Sized Objects

The device incorporating a needle, heater (2D910B1 silicon diode chip), and nanotweezer was assembled and connected to the electronic control circuit (Fig. 12). A shell-type heater is compatible with commercial Kleindiek manipulators. The photomicrograph of the nanotweezer located on the heater needle is presented in Fig. 13.

Similar manipulators made it possible to carry out experiments with the manipulation of real submicrometer-sized objects, namely, the whiskers of quasi-1D TaS_3 and NbS_3 conductors exhibiting the generation of charge-density waves (CDWs) [19]. The whiskers are micro- and nanofilaments whose thicknesses are usually less than 10 μm. Moreover, the minimum transverse sizes thereof are commonly limited by the possibilities of their detection, transport on a sub-

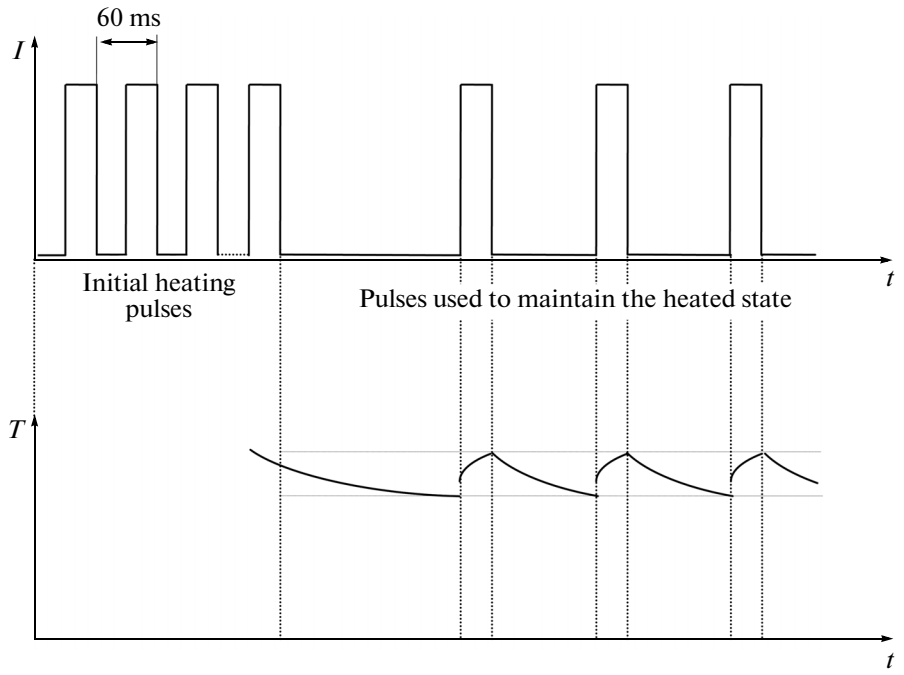

Fig. 10. Dependences of the current I and temperature T on the pulsed heating time upon controlling the SME microdevice.

strate, and mounting of contacts between them. As a rule, these operations are performed manually with the use of optical microscopes. In this case, the professional skill and acquired habits of specialists enables the investigation of the samples up to ~10 nm wide at a 1-μm distance between contacts. Such structures necessitate many efforts during preparation thereof. In addition, it should be noted that these efforts proved their value via the detection of several size effects observed only in the samples of the given kind (see [20] and references therein): the quantization of states, mesoscopic fluctuations of a threshold field, the coherent sliding of CDWs, the microwave field-induced synchronization of sliding [19], ultrahigh current densities of CDWs, etc. Suspended quasi-1D conductor samples can operate as unique self-sensitive torsion resonators [21, 22]. As might be expected, the fundamental resonance frequency increases to 1 GHz or more if the suspended part length varies down to 1 μm.

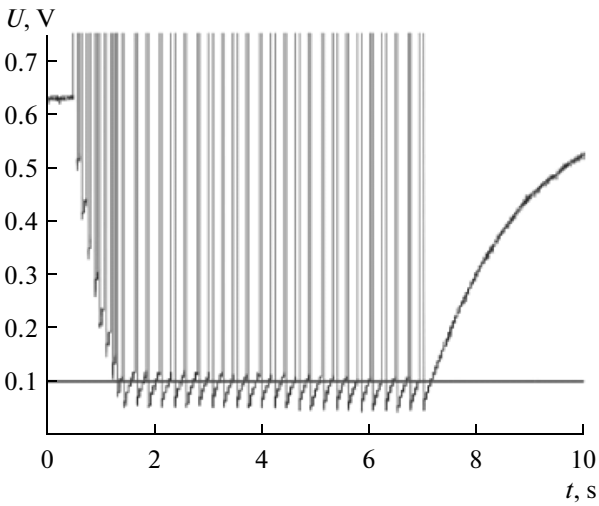

Fig. 11. Time dependence of the heating-element diode voltage when the microdevice control system is tested under pulse-periodic conditions. It is shown that, in the measurement range, the diode voltage diminishes with increasing temperature. After achieving the working temperature, the average diode voltage is stabilized at a level of 0.1 V (horizontal line).

In compliance with the aforementioned circumstances, a rather urgent problem is the nanowhisker-based manipulation of samples with CDWs and the preparation of their contacts under the condition that such operations are governed, e.g., with the help of a scanning electron microscope. During the experiment, an individual filamentary NbS_3 crystal was extracted from the total growth zone (Fig. 14a) and transported on another substrate. To measure the resistivity, the chosen whisker ends were fastened on two contact areas via ion-beam deposition of platinum (Fig. 14b). Subsequent measurements demonstrated a good quality of contacts.

3. DISCUSSION OF THE RESULTS

Approximate calculations based on the proposed model provided the results formulated as scaling rela-

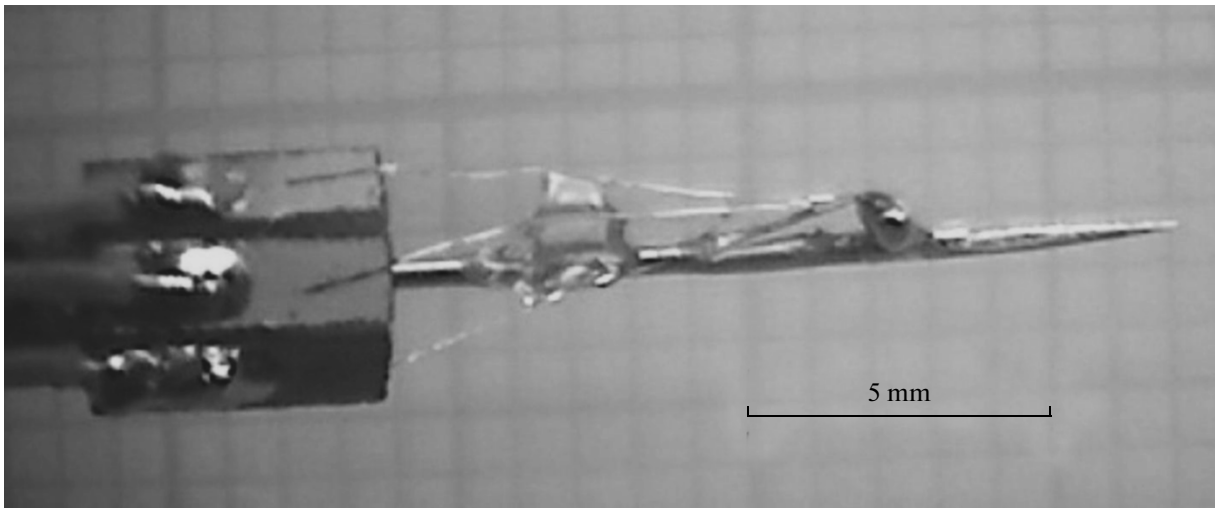

Fig. 12. Photomicrograph of the heater with a heating element (diode) fastened near the thin needle end.

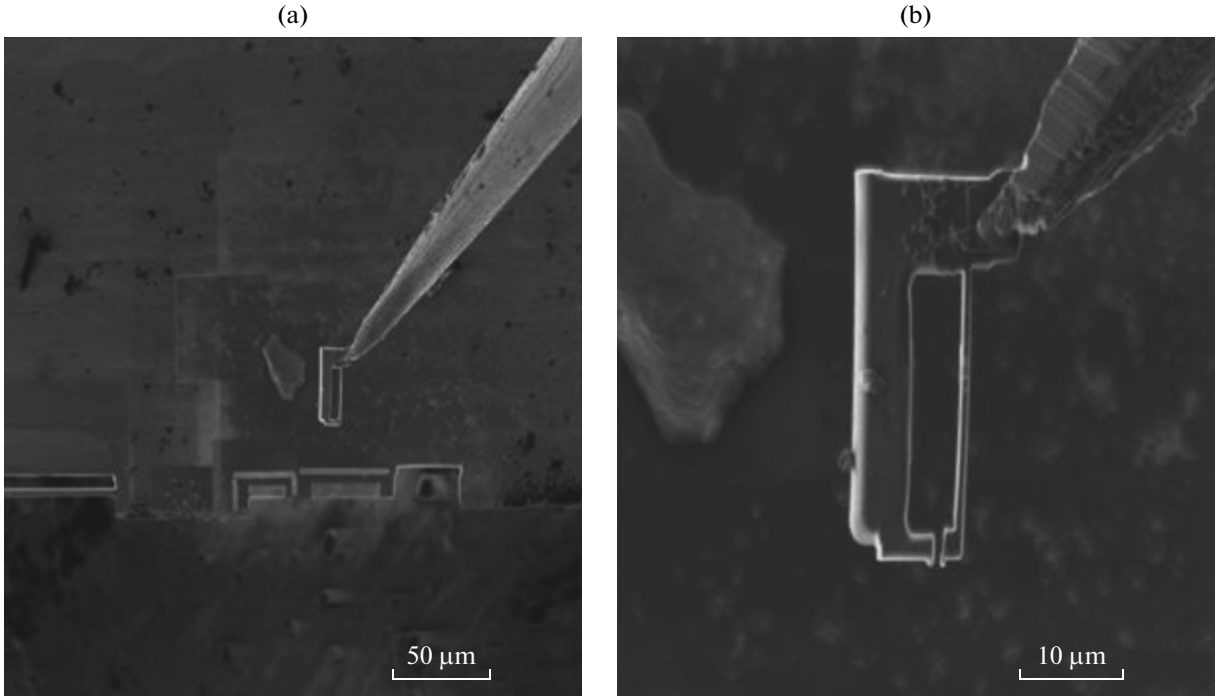

Fig. 13. Photomicrographs of the nanotweezer located at the heater needle end: (a) 1000× and (b) 5000× magnifications.

tionships (5)–(7) that imply a very fast increase in the speed of operation and decrease in the required energy $W \sim h^{-2.59}$, which obeys the power law. From these relationships, it follows that, in practice, the required control-pulse energy can be expected to reduce to 10^{-7}–10^{-8} J and the actuation time, to 10–1 μs. However, it is pertinent to note that the application of (5)–(7) involves the following severe difficulties of technological and fundamental physical nature:

(i) At present, fundamental physical restrictions imposed on the martensitic phase-transition rate and the SME arising from its excitation are unknown.

(ii) The scaling relationship $W \sim h^{-2.59}$ is valid only under pulsed heating conditions. When a continuous pulse train is prolonged, a nanotweezer does not cool and open. Such a situation is analogous to energy consumption in analog and digital electronics. To ensure

(a)

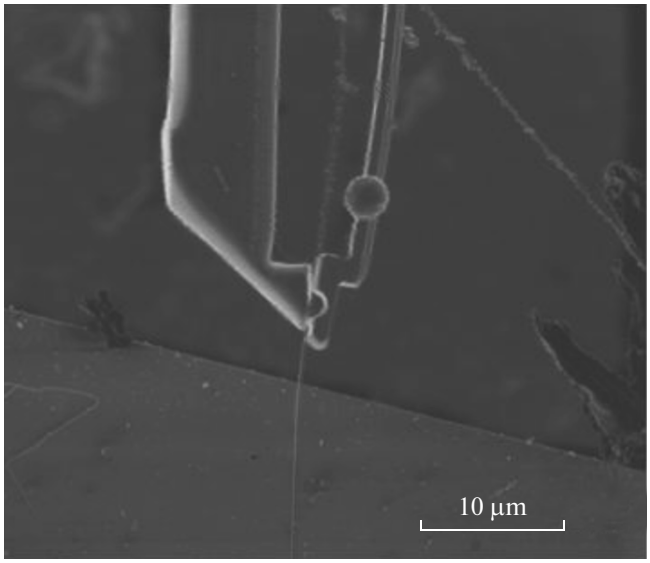

(b)

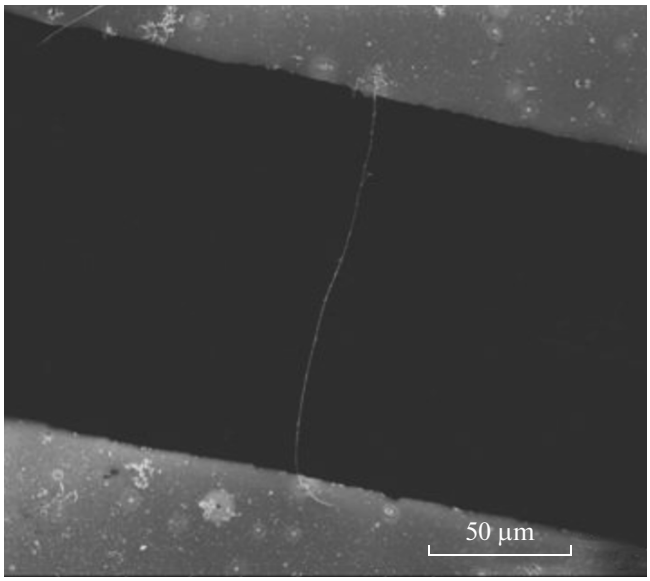

Fig. 14. Manipulation of the real submicrometer-sized object (quasi-1D TaS_3 whisker): (a) whisker is captured by the nanotweezer and (b) TaS_3 nanowhisker transported on the contact area.

that the nanotweezer's control system consumes energy only under changes from one state to another, its structure must correspond to the normally closed state. In this case, the object remains captured by the nanotweezer without expenditure of energy over an unrestrictedly long period of time and its liberation occurs upon arrival of the next pulse.

(iii) The basic system constraint preventing the implementation of high-speed nanomanipulations is the low imaging frequency in modern observation instruments: electron and ion microscopes.

CONCLUSIONS

The main results of the given study can be formulated as follows.

(i) The model intended to control a thermally activated micromechanical device with the shape memory effect, which is located at the tapered needle end, is proposed. The given model allows for the heat exchange between a needle and a heater and the heat removal near its base and enables us to calculate the durations of heating from the initial to actuation temperature of the device (i.e., to that of the martensite–austenite transition) and returning to the initial state (cooling to the austenite–martensite transition temperature). The technological restrictions on the maximum allowable heater temperature are chosen. The geometric sizes are scaled in the admissible range of cutting-edge technology: from 10 mm to 10 μm.

(ii) Numerical calculations indicate that the actuation time diminishes from 6.5 ms to 1.45 μs and the energy consumption, from 1.85×10^{-3} to 1.3×10^{-8} J, with decreasing sizes of the heating element arranged at distances of 10 mm to 10 μm from the tip of the standard tungsten needle 0.5 mm thick.

(iii) The control system of the SME nanotweezer mounted at the tungsten needle tip, which is compatible with a Kleindiek manipulator, is experimentally implemented. The pulse-periodic temperature-control mode makes it possible to turn on the heater, maintain the temperature and the nanotweezer's closed state, and turn off the heater by an operator command. The manipulation of real micrometer-sized objects is discussed.

(iv) From the result of our study, it is possible to define the scaling principle applied to thermomechanically controlled micro- and nanomechanical devices, which predicts that gradually decreasing sizes (from 1 mm to 10 μm) can lead to a power-law increase in the speed of operation and the same decrease in energy required for nanomechanical-device actuation. According to the derived scaling principle, the efficiency of promising nanorobotic systems can be improved sharply and their energy consumption diminished in passing to the technology ensuring the smaller geometrical sizes of the heating system.

ACKNOWLEDGMENTS

This study was supported by the Russian Foundation for Basic Research, project no. 14-19-01644.

REFERENCES

1. D. A. Gunderov, A. Lukyanov, E. A. Prokofiev, et al., Mater. Sci. Eng., A **503** (1–2), 75 (2009).
2. A. D. Bozhko, A. N. Vasil'ev, V. V. Khovailo, et al., Pis'ma Zh. Eksp. Teor. Fiz. **67**, 214 (1998).
3. A. D. Bozhko, A. N. Vasil'ev, V. V. Khovailo, et al., Zh. Eksp. Teor. Fiz. **115**, 1740 (1999).

4. A. A. Cherechukin, I. E. Dikshtein, D. I. Ermakov, et al., Phys. Lett. A **291**, 175 (2001).
5. V. D. Buchelnikov, I. E. Dikshtein, R. M. Greshichkin, et al., J. Magn. Magn. Mater. **272–276**, Pt. 3, 2025 (2004).
6. N. I. Kourov, A. V. Korolev, V. G. Pushin, et al., Phys. Met. Metallogr. **99**, 376 (2005).
7. V. G. Pushin, N. I. Kourov, A. V. Korolev, et al., Phys. Met. Metallogr. **99**, 401 (2005).
8. E. Kalimullina, A. Kamantsev, V. Koledov, et al., Phys. Status Solidi **11**, 1023 (2014).
9. A. Irzhak, V. Koledov, D. Zakharov, et al., J. Alloys Compd. **586** (Suppl. 1), 464 (2014).
10. K. Akatyeva, V. Afonina, F. Albertini, et al., Solid State Phenom. **190**, 295 (2012).
11. D. Zakharov, G. Lebedev, A. Irzhak, et al., Smart Mater. Structures **21**, 052001 (2012).
12. A. V. Shelyakov, N. N. Sitnikov, V. V. Koledov, et al., Int. J. Smart Nano Mater. **2** (2), 68 (2011).
13. A. V. Shelyakov, N. N. Sitnikov, A. P. Menushenkov, et al., Thin Solid Films **519**, 5314 (2011).
14. D. Zakharov, G. Lebedev, V. Koledov, et al., Phys. Procedia **10**, 58 (2010).
15. A. V. Irzhak, D. I. Zakharov, V. S. Kalashnikov, V. V. Koledov, D. S. Kuchin, G. A. Lebedev, P. V. Lega, E. P. Perov, N. A. Pikhtin, V. G. Pushin, I. S. Tarasov, V. V. Khovailo, V. G. Shavrov, and A. V. Shelyakov, J. Commun. Technol. Electron. **55**, 818 (2010).
16. A. V. Irzhak, V. S. Kalashnikov, V. V. Koledov, D. S. Kuchin, G. A. Lebedev, P. V. Lega, N. A. Pikhtin, I. S. Tarasov, V. G. Shavrov, and A. V. Shelyakov, Tech. Phys. Lett. **36**, 329 (2010).
17. A. N. Tikhonov and A. A. Samarskii, *Equations of Mathematical Physics* (Mosk. Gos. Univ., Moscow, 2004; Pergamon Press, Oxford, 1964).
18. L. K. Martinson and Yu. I. Malov, *Differential Equations of Mathematical Physics* (Bauman MGTU, Moscow, 2002) [in Russian].
19. V. Ya. Pokrovskii, S. G. Zybtsev, M. V. Nikitin, et al., Usp. Fiz. Nauk **183**, 33 (2013).
20. S. V. Zaitsev-Zotov, Usp. Fiz. Nauk **174**, 585 (2004).
21. M. V. Nikitin, V. Ya. Pokrovskii, and S. G. Zybtsev, Zh. Radoelektron., No. 2, (2013); http://jre.cplire.ru/jre/feb13/8/text.pdf).
22. V. Ya. Pokrovskii, M. V. Nikitin, and S. G. Zybtsev, Physica B **460**, 39 (2015).

Translated by S. Rodikov